Self-Motion Analysis of Extensible Continuum Manipulators

Apoorva D. Kapadia* and Ian D. Walker

Abstract—While the field of continuum manipulators has been the subject of increasing attention from the robotics community, knowledge of their inherent capabilities is still limited. Controllers have been proposed that exploit the null-space of redundant continuum manipulators, however studies of the nature of continuum robot null-spaces have not yet been done. In this paper, we first develop a convenient set of extensible, continuum manipulator forward kinematics and resolved-motion rate inverse kinematics. This allows us to analyze the null-space of 2-section, planar, extensible, redundant continuum manipulators to consider the underlying structure of general continuum robot self-motions and discuss their importance to real-world examples and applications.

I. Introduction

Continuum robots, or robots with continuous backbones are receiving greater attention within the robotics community, a comprehensive overview for which can be found in [1], [2], [3]. The design of these manipulators have been inspired by elements of the Animal Kingdom [4] and are unique in their ability to perform tasks and functions that are not possible or are too complicated for conventional robots. This is because of a continuum manipulator's inherent features of structural compliance and bending at any point along its length. The more commonly identifiable tasks are navigation in congested environments and whole-arm grasping. Whole arm grasping, as the name suggests, is when the robot takes advantage of its kinematic redundancy to curl around objects and uses its body structure (as opposed to a gripper) for manipulation. This allows for manipulable objects to have a variety of shapes, sizes and physical properties. Numerous continuum manipulator designs have been proposed [2], [5], [6], [7], [8], [9], [10], [11].

Kinematic models for continuum manipulators can be considered to be well understood and have been developed in [12], [13], [14], [15]. Continuum manipulator dynamics have been derived in [16], [17], [18] and is an area of active research. The dynamics by Tatlicioglu *et al.* are based on the kinematics in [14]. Configuration-space controllers for continuum manipulators have been proposed by [19], [20], [21], [22], [23], while a task-space controller was developed by [24] and a teleoperation controller in [25].

While mathematical models and controllers for continuum manipulators have been investigated, one area that has not yet been studied in detail is the manipulator null-space.

Burdick [26] analyzed the null-space of rigid-link redundant manipulators, characterizing them as a set of disjoint manifolds based on the sets of possible configurations as a result of the redundant manipulator's self-motion property. Burdick categorized the null-space for conventional redundant rigid-link manipulators, but this does not apply to continuum robots as there are inherent structural differences between rigid-link and continuum manipulators (which are conceptually like strings, but have physical constraints on their motion). Similar analyses to that in [26] for continuum manipulators, to the best of our knowledge, do not exist, thus the work presented here attempts to gain a better understanding of the null-space of general continuum manipulators, focusing on the core capabilities of 2-section, redundant, extensible continuum manipulators.

We characterize the manipulator self-motion into three types i) Self-motion due to bending, ii) Self-motion due to extension, and iii) General motion case (shown herein to be a combination of the previous two cases). We begin by describing a convenient set of 3D forward kinematics for a 2-section extensible continuum manipulator in Section II. In Section II-C, we discuss the inherent structural differences between the self-motion manifolds for rigid-link redundant manipulators, and their counterpart in continuum robots. Section III-A details the velocity kinematics and the subsequent resolved motion-rate inverse kinematics, based on the method first proposed by [27] leading to a completely new null-space characterization for continuum manipulators.

Controllers proposed for extensible continuum robots have focused on the control of the shape of the manipulator or the control of the tip at an arbitrary location with additional sub-tasks. These works implicitly deal with the null-space, but do not utilize (or are not able to take advantage of the structure of) the null-space itself. This paper fills that gap by analyzing the motion of the continuum manipulator sections when the tip is fixed at an arbitrary point. This is important for numerous applications and is discussed in Section IV.

II. Global Kinematics

The general forward kinematics for a manipulator with $n-$degrees of freedom (DOF) are given by

$$x = f(\psi), \tag{1}$$

where $x(t) \in \mathbb{R}^m$ represents the task-space coordinates of the manipulator tip, $f(\cdot) : \mathbb{R}^n \to \mathbb{R}^m$ represents the manipulator forward kinematics, and $\psi(t) \in \mathbb{R}^n$ is the set of configuration-space variables (comprising each internal degree of freedom)

for the manipulator. When $n > m$, the manipulator is considered to be kinematically redundant.

Continuum manipulators are flexible and compliant robots that can theoretically bend in any direction at any point along their length. Practically however, continuum backbones, which theoretically have infinite degrees of freedom, need to be realized robotically using a small (finite) number of actuators. The degrees of freedom not directly controlled must be constrained in the design in order to produce predictable behavior. In all continuum robots to date, this design constraint results in the robot being a series of serially connected "sections", which can bend (typically in 2 dimensions) and often extend/contract. While numerous physical instantiations of continuum robots have appeared [10], [11], [28], [29], in all but one case [30], the designs result in sections which are constrained to approximately constant curvature [1], [2], [3]. Thus, constant curvature section continuum robots is the case analyzed in this paper.

Physical artifacts consist of serially connected continuum sections allowing for bending in multiple directions to accomplish more complex tasks. Unlike rigid-link redundant robots, where the kinematics are based on the joint angles between links ($\theta(t)$) or their extensibility ($d(t)$), continuum manipulators are represented by the length of the arc each section subtends ($s(t)$), the curvature of the arc ($k(t)$), and the angle of curvature ($\phi(t)$) as detailed in Figure 1 and Figure 2

Consider a spatial two-section extensible continuum robot as shown in Figure 1, where $X_i(t)$, $Y_i(t)$, and $Z_i(t) \in \mathbb{R}$
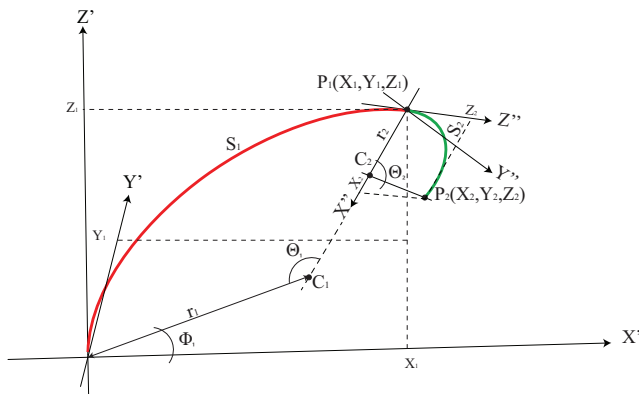

Fig. 1. 3-Dimensional Schematic of a Two-Section Octarm

represent the coordinates of the tip of each robot section in the local frame[1], and with each set collectively represented by $\boldsymbol{P_i(t)} \in \mathbb{R}^3$; $s_i(t)$, $\kappa_i(t)$, and $\phi_i(t) \in \mathbb{R}$ represent the section length, section curvature, and section angle of curvature respectively; $r_i(t) \in \mathbb{R}$ is the section radius while $C_i(t) \in \mathbb{R}$ represents the center of the circle in the local frame of which each section is a part and is always on the $\boldsymbol{X_i Z_i}$-plane of the local frame; $\theta_i \in \mathbb{R}$ represents the angle subtended by the arc of the section in the local frame; and $X(t)$, $Y(t)$, and $Z(t) \in \mathbb{R}$ represent the coordinates of the tip

[1]In all cases, $i = 1, 2$ representing the first or second sections of the continuum robot respectively

of the second section with respect to the base frame, while $\boldsymbol{X'Y'Z'}$ represent the coordinate frame of the first section and $\boldsymbol{X''Y''Z''}$ represent the coordinate frame of the second section with respect to the top of the first section. It can be seen that

$$\begin{aligned} \theta_i(t) &= s_i(t)\kappa_i(t) \\ \kappa_i &= r_i(t)^{-1} \end{aligned} \tag{2}$$

Remark 1: It is assumed that the variables $s_i(t)$, $\kappa_i(t)$, and $\phi_i(t)$ are measureable and each section bends with uniform curvature, resulting in the arcs being parts of circles with radius $r_i(t) = \kappa_i(t)^{-1}$.

Remark 2: For the kinematic analysis, the coordinate axes are set up at the base of each section such that each manipulator section curves tangentially to one of the local coordinate axes. This constraint is inherited directly from the implementation of physical continuum robots [4] which must bend about an initial (locally fixed) tangent. In this paper, the kinematics are developed for the sections curving tangential to the positive Z_i axes. The subsequent kinematics can also be developed with the sections tangential to the local $\pm X_i$ axes or $-Z_i$ axis by simply modifying the rotation matrices as needed.

A. Base Section Kinematics

Figure 2 shows the robot in the (X'Z') plane (in which the first section lies entirely). In that figure, consider the $\triangle C_1 P_1 X_1$, where it can be seen that $\angle P_1 C_1 X_1 = (\pi - \theta_1)$ and $\angle P_1 X_1 C_1 = 90^o$. Also, $\bar{C_1 P_1} = r_1$ and $\bar{C_1 X_1} = X_1 - r_1$, which can be utilized to give

$$cos\,(\pi - \theta_1) = \frac{X_1 - r_1}{r_1}. \tag{3}$$

The expression in (3) can be rewritten as

$$X_1 = r_1 - r_1 cos\,(\theta_1)\,, \tag{4}$$

and using the expression in (2) in (4) results in

$$X_1 = \frac{1 - cos\,(\theta_1)}{\kappa_1}. \tag{5}$$

Similarly, the dual trigonometric expression that can be used from the same triangle results in

$$\frac{Z_1}{r_1} = sin\,(\pi - \theta_1)\,, \tag{6}$$

which can be rewritten as

$$Z_1 = \frac{sin\theta_1}{\kappa_1}. \tag{7}$$

To calculate the Y_1-coordinate, the arm section is rotated counterclockwise around the Z_1-Axis by an angle $\phi_1 \in \mathbb{R}$. Thus the 2D (X_1, Z_1) coordinates in (5) and (6) are converted into 3D (X_1, Y_1, Z_1) by

$$P_{1-3D} = \begin{bmatrix} cos\phi_1 & -sin\phi_1 & 0 \\ sin\phi_1 & cos\phi_1 & 0 \\ 0 & 0 & 1 \end{bmatrix} \begin{bmatrix} \frac{1-cos(\theta_1)}{\kappa_1} \\ 0 \\ \frac{sin(\theta_1)}{\kappa_1} \end{bmatrix}, \tag{8}$$

where the matrix represents the 3D Z-axis rotation, resulting in

$$P_{1-3D} = \begin{bmatrix} X_1 \\ Y_1 \\ Z_1 \end{bmatrix} = \frac{1}{\kappa_1} \begin{bmatrix} cos(\phi_1)(1-cos(\theta_1)) \\ sin(\phi_1)(1-cos(\theta_1)) \\ sin(\theta_1) \end{bmatrix}. \quad (9)$$

Given the constraint of the initial tangent coinciding with Z_1, it should be noted that the forward kinematics in (9) are unique for a single section in either the spatial or planar (when $\phi(t) = 0$, see Figure 3(b)) cases. The implications of this are discussed in further detail in Section II-C.

B. Second Section Kinematics

In the local frame, the kinematics derivation of the second section is identical to that of the base section by considering $\triangle C_2 P_2 X_2$. This results in the local frame coordinates of the tip of the second section to have the form

$$P_{2-3D} = \begin{bmatrix} X_2 \\ Y_2 \\ Z_2 \end{bmatrix} = \frac{1}{\kappa_2} \begin{bmatrix} cos(\phi_2)(1-cos(\theta_2)) \\ sin(\phi_2)(1-cos(\theta_2)) \\ sin(\theta_2) \end{bmatrix}. \quad (10)$$

In order to represent the coordinates of the second section tip in the world frame, the second section coordinates have to be first rotated clockwise by the angle $\theta_1(t)$ about the Y_1-axis, rotated again (counterclockwise) by the angle $\phi_1(t)$ about the Z_2 axis and finally added to the coordinates of the first section tip. Thus the 3D coordinates of a two-section continuum manipulator are given by

$$\begin{bmatrix} X \\ Y \\ Z \end{bmatrix} = \begin{bmatrix} X_1 \\ Y_1 \\ Z_1 \end{bmatrix} +$$
$$\begin{bmatrix} cos\phi_1 & -sin\phi_1 & 0 \\ 0 & cos\phi_1 & 0 \\ sin\phi_1 & 0 & 1 \end{bmatrix} \begin{bmatrix} cos\theta_1 & 0 & sin\theta_1 \\ 0 & 1 & 0 \\ -sin\theta_1 & 0 & cos\theta_1 \end{bmatrix} \begin{bmatrix} X_2 \\ Y_2 \\ Z_2 \end{bmatrix} \quad (11)$$

If $\phi_1(t) = \phi_2(t) = 0$, manipulator motion is restricted to the X-Z plane, as shown in Figure 2, and this case will be the main consideration for the rest of this article. This results in the coordinates of the tip being represented by $[X(t) \; Z(t)]^T$, where

$$\begin{aligned} X &= \frac{1}{k_1} - \frac{1}{k_1}cos\theta_1 + \frac{1}{k_2}cos\theta_1 - \frac{1}{k_2}cos\theta_1cos\theta_2 \\ &\quad + \frac{1}{k_2}sin\theta_1sin\theta_2; \\ Z &= \frac{1}{k_1}sin\theta_1 - \frac{1}{k_2}sin\theta_1 + \frac{1}{k_2}sin\theta_1cos\theta_2 \\ &\quad + \frac{1}{k_2}cos\theta_1sin\theta_2, \end{aligned} \quad (12)$$

C. Self-Motion Manifolds

As discussed in the introduction, we are interested in categorizing the self-motion of continuum robots, *i.e.* the type and nature of internal movement where the tip remains at a fixed location. The underlying structures describing self-motion topologically are self-motion manifolds [26]. Self-motion manifolds group the infinity of inverse kinematic solutions into a finite and bounded set of solutions. Understanding of these solutions enables practical exploitation of
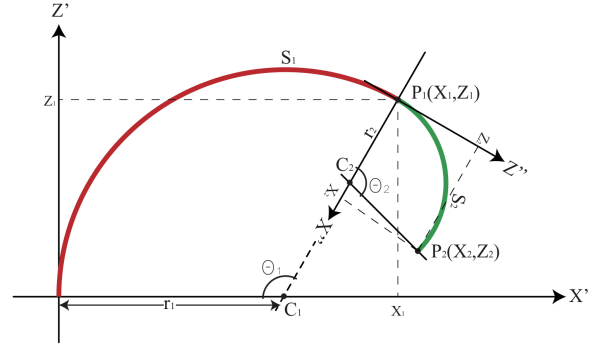

Fig. 2. Planar Schematic of two-section Octarm

the manipulator self-motion. In this section, we discuss the "self-motion manifolds" inherent for continuum robots.

Self-motion manifolds of redundant manipulators have been categorized in [26]. However, the manipulators in question were rigid-link and revolute. For these manipulators, the analysis in [26] resolves the fundamental question of how many distinct self-manifolds exist (physically, how many distinct self-motions exist). In [26], it is shown that for serial rigid-link revolute manipulators, there are up to 16 potential distinct self-motion solutions. As the number of rigid links increase, the number of self motions decreases, until they resemble "strings" having only one self-motion solution.

As noted in Section II, serially-connected continuum sections bend to resemble "strings" more so than their rigid-link counterparts. However the physical constraints continuum manipulators have in comparison to strings are significant. Thus since continuum manipulator motion capabilities lie in between that of redundant rigid-link robots and strings, a deeper understanding is required.

For rigid-link manipulators, it is shown in [26] that there exist two distinct types of pose-based self-motion manifolds, physically corresponding to different self-motions from the "elbow up" and "elbow-down" configurations for the same position as shown in Figure 3(a). Multiple self-motion manifolds arise because, for some end-effector locations, there are disjoint "elbow-up" and "elbow-down" trajectories which cannot cross into each other. Such crossings occur at singular configurations. It is shown by induction in [26] that there is an upper limit (that number being 10) of distinct self-motions manifolds. However, for continuum robots the solution is quite different. In fact, the following result holds:

Theorem 1: There is a single unique self-motion manifold for serially connected continuum manipulators.

Proof: Consider a single section continuum robot. As stated in Remark 2, there exists a constraint for the initial tangent to be fixed. This constraint, along with the constant curvature assumption implies that there is a unique configuration for any tip location. Thus, it can be seen that the "elbow up" and "elbow down" configurations of rigid-link robots (shown in Figure 3(a)) do not have equivalent feasible

inverse kinematic solutions for continuum manipulators. The "elbow down" equivalent of the continuum manipulator base section is possible only with a different initial mounting (180° from that shown in Figures 1 and 2)), and shown in Figure 3 (right).
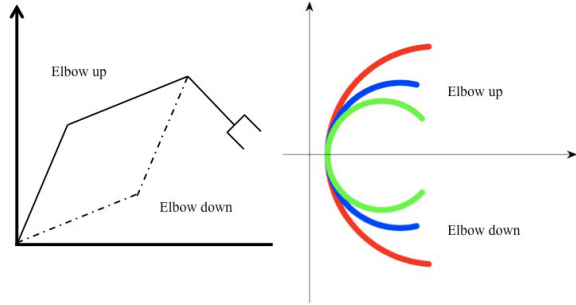

Fig. 3. Left: The "elbow-up" and "elbow-down" configurations for rigid-link robots as described in [26]. Right: The equivalent for continuum robots only possible by redefining the kinematic equations as described in Theorem 1.

Now consider a 2-section continuum manipulator. Let $\mathbb{C}$ denote the set of locations formed by the point $\mathbb{D}$ connecting the two solutions when moving section 2 and keeping the tip fixed. Each point in $\mathbb{C}$ corresponds uniquely to a configuration of section 2 ($\mathbb{D}$ to tip) and also uniquely to a configuration of section 1 (base to $\mathbb{D}$) since each section has a unique $1-1$ kinematic map, as shown in Figure 4. Thus, any self-motion trajectory corresponds to a unique self-motion trajectory, and hence a single self-motion manifold.
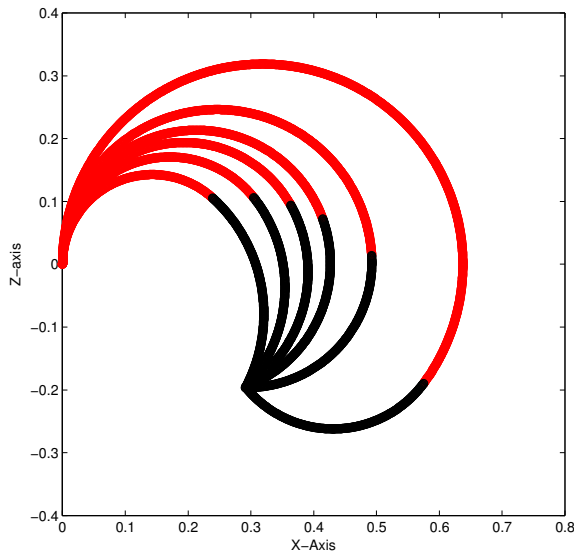

Fig. 4. The 2-section continuum manipulator, showing a $1-1$ kinematic map for the point connecting sections 1 and 2.

By induction, it can be seen that there is only one self-motion manifold for any serially connected, constant curvature, multi-section continuum robot. ∎

The self-motion manifold for continuum manipulators, unlike their rigid-link counterpart, is also not hindered by singu-

larities. This is because singular configurations exist only when each manipulator section is straight along the axis its base is tangential to, resulting in the curvature $k(t) = 0$. This lack of singularities within the rest of the configuration-space results in self-motion solutions easily "traveling into" one another as opposed to being divided by a loci of singularities in the rigid-link cases.

III. THE NULL-SPACE: LOCAL ANALYSIS

A. Velocity Kinematics

A two-section extensible continuum manipulator as seen in Figure 2 is kinematically redundant for 3D (X-Y-Z) positioning tasks in 3D space as it has 6 DOFs. Redundancy also exists for the XZ planar positioning case (by setting $\phi_1(t) = \phi_2(t) = 0$), since 4 DOFs still exist ($s_1(t)$, $k_1(t)$, $s_2(t)$, and $k_2(t)$).

Given that the manipulator is redundant, the inverse kinematics for the manipulator yield non-unique solutions. This means that there exist infinite manipulator configurations for the same position of the manipulator tip. Thus the manipulator configuration cannot be conveniently computed from positional inverse kinematics. Due to this, we utilize the manipulator velocity kinematics.

The velocity kinematics for the planar extensible continuum manipulator are obtained by taking the time derivative of the kinematic model, and are given by

$$\dot{x} = J\left(\psi\right)\dot{\psi}, \qquad (13)$$

where $J(\cdot) \in \mathbb{R}^{m \times n}$ is the Jacobian matrix defined by

$$J = \frac{\partial f(\cdot)}{\partial \psi}, \qquad (14)$$

and $\dot{x}(t) \in \mathbb{R}^m$ represents the task-space velocity, and $\dot{\psi} \in \mathbb{R}^n$ represents the configuration-space velocity. For a 4 DOF extensible continuum manipulator in the $X - Z$ plane, the velocity Jacobian is found to be

$$J \triangleq \begin{bmatrix} \frac{\partial X}{\partial s_1} & \frac{\partial X}{\partial k_1} & \frac{\partial X}{\partial s_2} & \frac{\partial X}{\partial k_2} \\ \frac{\partial Z}{\partial s_1} & \frac{\partial Z}{\partial k_1} & \frac{\partial Z}{\partial s_2} & \frac{\partial Z}{\partial k_2} \end{bmatrix}. \qquad (15)$$

B. Resolved Motion Rate Inverse Kinematics

To numerically solve the inverse kinematics problem for non-redundant manipulators in the velocity domain, an initial motion is fed on both sides of (13) to be multiplied by $J(\cdot)^{-1}$ (when $[J]^{-1}$ is defined and invertible) resulting in

$$\dot{\psi} = [J]^{-1}\dot{x}. \qquad (16)$$

The expression in (16) can then be numerically integrated to obtain $\psi(t)$. This method of obtaining a robot configuration from the velocity kinematics is known as the "resolved-motion rate" approach [27].

However, for kinematically redundant manipulators, $J(\cdot)$ is never square, in which case matrix inversion is not directly possible. Thus the Moore-Penrose pseudoinverse of $J(\cdot)$, given by $J^+(\cdot) = J^T \left(J J^T\right)^{-1} \in \mathbb{R}^{n \times m}$ is often utilized. The

pseudoinverse $J^+(\cdot)$ satisfies $JJ^+ = I_m$ where I_m is the $m \times m$ identity matrix. Properties of the Moore-Penrose Pesudoinverse can be found in [31]. For kinematically redundant manipulators, the inverse kinematics solution in the velocity space can be given by

$$\dot{\psi} = [J]^+ \dot{x}. \qquad (17)$$

Along with finding a specific inverse kinematic solution for redundant manipulators, it is also important for us to characterize all the solutions. Thus, we modify the pseudoinverse solution, (17) as

$$\dot{\psi} = [J]^+ \dot{x} + [I_n - J^+ J] \epsilon, \qquad (18)$$

where $I_n \in \mathbb{R}^{n \times n}$ is the $n \times n$ identity matrix, and $\epsilon \in \mathbb{R}^{n \times 1}$ is an arbitrary vector. Both terms on the right side of (18) represent joint velocities, and can be further denoted as

$$\dot{\psi} = \dot{\psi}_P + \dot{\psi}_N, \qquad (19)$$

where $\dot{\psi}_P \in \mathbb{R}^{n \times 1}$ represents the particular solution and $\dot{\psi}_N \in \mathbb{R}^{n \times 1}$ represents the homogeneous solution, given by

$$\begin{aligned} \dot{\psi}_P &= [J]^+ \dot{x} \\ \dot{\psi}_N &= [I_n - J^+ J] \epsilon \end{aligned} \qquad (20)$$

The homogeneous solution refers to the fact that $[J]\dot{\psi}_N = 0$, i.e. solutions $\dot{\psi}_N$ (parameterized by the arbitrary ϵ) are joint velocities that produce no tip motion, and thus characterize the self-motion.

Thus, to better explore the self-motion of an extensible continuum manipulator, we calculate its Jacobian null-space and analyze manipulator motion in that space. To that end, we begin with the planar 2-section extensible continuum robot, for which the null-space matrix, denoted by $\xi_N(t) \in \mathbb{R}^{4 \times 4}$, is defined as

$$\xi_N \triangleq I_4 - J^+ J, \qquad (21)$$

where $I_4 \in \mathbb{R}^{4 \times 4}$ represents an identity matrix, and $J^+(\cdot) \in \mathbb{R}^{4 \times 2}$ is the Moore-Penrose pseudoinverse of the Jacobian matrix, $J(\cdot)$. The columns (or rows) of $\xi_N(t)$ span the null space in $\mathbb{R}^4$.

IV. SELF-MOTION CHARACTERIZATION

To better understand the self-motion behavior of continuum manipulators we consider 3 cases for 2-section extensible continuum robots:

1) Constant second section curvature case;
2) Constant second section length case; and
3) General motion case.

In case 1 and case 2, the constant curvature and length respectively represent restrictions on curvature and length of the second section only. In all cases the first section is free to move without any constraints while the manipulator tip remains fixed at its initial point. No physical restrictions have been placed on the manipulator section lengths or curvatures except $s_i(t) > 0$ and $r_i(t) > 0$ (*i.e.* $k_i(t) < \infty$).

A. Self-Motion Due To Extension

In this case, the first section has no constraints on its length or curvature while the length of the second section is free to change with its curvature being fixed, as seen in Figure 5 and the associated video. Further, it can be seen that the overall shape of the manipulator remains the same despite the changes in section lengths. This is probably the most intuitive self-motion case.
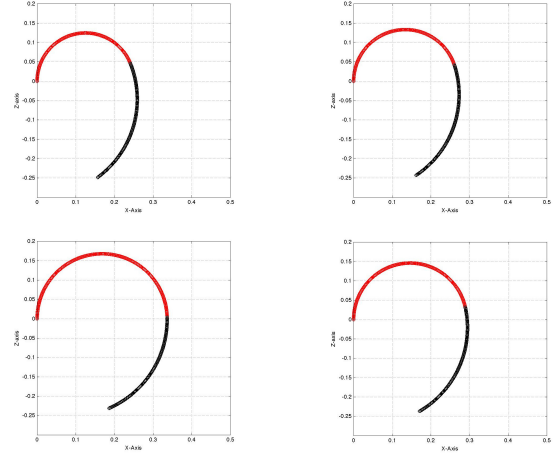

Fig. 5. Screenshots from the accompanying video of the constant second section curvature case. The time lapse is clockwise starting from the top left.

Based on (18), the velocity kinematics for this case can be given by

$$\dot{\psi}_{cc} = \begin{bmatrix} \dot{s_1} \\ \dot{k_1} \\ \dot{s_2} \end{bmatrix} = [J_{cc}]^+ \dot{x} + [I_3 - J_{cc}^+ J_{cc}] \epsilon, \qquad (22)$$

where $\dot{\psi}_{cc}(t) \in \mathbb{R}^4$ represents the configuration space velocity, $J_{cc}(t) \in \mathbb{R}^{2 \times 3}$ is the Jacobian for the second section constant curvature case, $J_{cc}^+(t) \in \mathbb{R}^{3 \times 2}$ is the pseudoinverse of $J_{cc}(t)$, and $\epsilon(t) \in \mathbb{R}^3$ is an arbitrary vector. It should be noted that since the curvature of the second section is constant, the $\frac{\partial X}{\partial k_2}$ and $\frac{\partial Z}{\partial k_2}$ from (15) are not used in $[J_{cc}]$ resulting in the $\dot{k_2}(t)$ term not present in the null-space vector $\dot{\psi}_{cc}(t)$.

An example in nature of the use of constant curvature 2-section continuum structures is the larvae of the *Ascidian* (also known as a Sea Squirt), *Distaplia occidentalis* [32], where McHenry found the the tails of free-swimming larvae were made up of two extensible sections. each section bent with constant curvature, and the curvatures and angles changed depending on the direction of motion.

B. Self-Motion Due to Bending

In this case, the curvature of the second section is variable while its length is kept constant and there are no restrictions on the base section. Figure 6 and video (see attached video) show this case, where the lengths of both the first and second sections vary while the curvature remains constant.
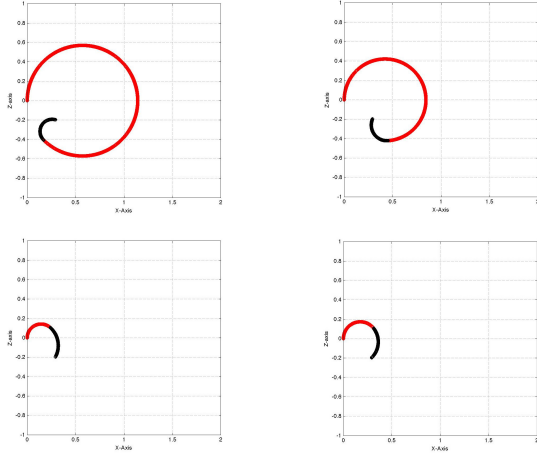
Fig. 6. Screenshots from the accompanying video of the constant second section length case. The time lapse is clockwise starting from the top left.

Based on (18), and parallel to (22) the velocity kinematics for this case can be given by

$$\dot{\psi}_{cl} = \begin{bmatrix} \dot{s_1} \\ \dot{k_1} \\ \dot{k_2} \end{bmatrix} = [J_{cl}]^+ \dot{x} + [I_3 - J_{cl}^+ J_{cl}] \epsilon, \qquad (23)$$

where $\dot{\psi}_{cl}(t) \in \mathbb{R}^3$ represents the configuration space velocity, $J_{cl}(t) \in \mathbb{R}^{2 \times 3}$ is the Jacobian for the second section constant curvature case, $J_{cl}^+(t) \in \mathbb{R}^{3 \times 2}$ is the pseudoinverse of $J_{cl}(t)$, and $\epsilon(t) \in \mathbb{R}^3$ is an arbitrary vector. It should be noted that since the length of the second section is constant, $\frac{\partial X}{\partial s_2}$ and $\frac{\partial Z}{\partial s_2}$ from (15) are not used in $[J_{cl}]$ resulting in the $\dot{s_2}(t)$ term not present in the null-space vector $\dot{\psi}_{cl}(t)$.

One application uniquely applicable to continuum manipulators is that of rolling an object. Mobile hospital units often need help turning a patient over, especially in cases of rehabilitation. In this case, a 2-section continuum manipulator could maneuver and around the the patient with the tip's location setting up it's fixed point under the patient. Using self-motion, the tip section would increase it's curvature to leverage the patient, while the base section reduces its length so as to pull the patient back, effectively rolling them over. This is analogous to the way nurses utilize their hands and arms to roll a patient over. To do so, the nurse would leverage their hands around and under the patient while standing on the other side. The nurse then pulls their hands out and back while leveraging the patient with their elbows to avoid slip and thus rolling the patient over in their bed.

C. The General Motion Case

We now consider the general selfmotion case allowing for the manipulator to be completely unrestricted in its motion.

Theorem 2: The general self-motion of planar 2-section extensible continuum manipulators is spanned by the constrained manipulator self-motion velocities.

Proof: The null-space vector in (22) can be viewed and expanded into $\mathbb{R}^4$ as

$$\psi_{cc} = \begin{bmatrix} \dot{s_{1_{cc}}} \\ \dot{k_{1_{cc}}} \\ \dot{s_{2_{cc}}} \\ 0 \end{bmatrix} \in N[J]. \qquad (24)$$

The last element of ψ_{cc}, nominally $\dot{k_2}(t)$ does not exist for this case (constant second section curvature) and thus its position is padded with a zero. Note that (24) remains a self-motion velocity for the manipulator, *i.e.* $[J]\psi_{ee} = 0$. Similarly, (23) can be expanded as,

$$\psi_{cl} = \begin{bmatrix} \dot{s_{1_{cl}}} \\ \dot{k_{1_{cl}}} \\ 0 \\ \dot{k_{2_{cl}}} \end{bmatrix} \in N[J], \qquad (25)$$

as the $\dot{s_2}(t)$ term does not exist, and therefore has no effect on the manipulator motion due the constant length second section case being considered, and is thus padded by a zero.

From the general inverse kinematic solution in (18) (valid through the workspace except for the infinitesimally thin subspaces of the local X and Z axes, *i.e.* $k_i(t) = \sigma$), for $[J(t)]$ of full rank 2, $[I - J^+ J]$ is of rank 2, and that the columns of $[I - J^+ J]$ span the null-space [33]. The general null-space is thus 2-dimensional, and given that the vectors in (24) and (25) are clearly both in $N[J]$ and independent, they form a basis for the null-space.

$$\psi = \begin{bmatrix} \dot{s_1} \\ \dot{k_1} \\ \dot{s_2} \\ \dot{k_2} \end{bmatrix}. \qquad (26)$$

Thus, we can see that (26) must result from a the linear combination of the vectors in (24) and (25),

$$\dot{\psi} = K_{cc}\dot{\psi}_{cc} + K_{cl}\dot{\psi}_{cl}, \qquad (27)$$

where $K_{cc}, K_{cl} \in \mathbb{R}$ are constants. ∎

An example of the general self-motion, generated using (27), in Figure 7 and video (see attached video), it can be seen that the both the first and second section lengths increase, and their curvatures decrease. Note the scale changes as a result of combining the two special cases.

One potential application for this case is on-sea refueling, with the ships lining up next to each other and a continuum robot hose being used for transmitting the fuel. Given that the ships are constantly in relative motion due to the active sea states, and the high pressure with which the fuel is being transmitted, it is imperative that the "hose" not flail about in the event of a disconnection, while the configuration be compliant. Exploitation of the manipulator null-space is necessary in such situations.

A novel way to apply continuum manipulators is using two continuum sections as a hand-finger equivalent with the hand and the finger distinguised from each other at the point where
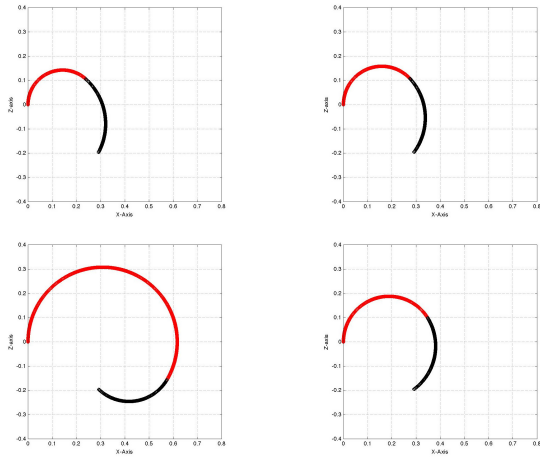
Fig. 7. Screenshots from the accompanying video of the fully variable second section case. The time lapse is clockwise starting from the top left.

the sections join. The constant curvature paradigm could be used for the hand in order to set leverage a tip position similar to a lasso winding around an object. The constant length self-motion and/or base section motion can then change its shape to manipulate the object as required.

V. CONCLUSION

In this paper we present new insight into and characterization of the self-motion properties of continuum robots. We show that there is a single self-motion manifold underlying the available self-motion. To that end, we develop a new, simplified set of forward kinematics for extensible continuum manipulators along with the resolved-motion rate inverse kinematics. This allows us to conveniently analyze the manipulator null-space in order to explore the self-motion characteristics of continuum manipulators. We identify 3 base self-motion cases which generate continuum manipulator behavior in the null-space and discuss the practical implications of these findings along with real-world examples or application in each case.

REFERENCES

[1] G. Robinson and J. Davies, "Continuum robots - a state of the art," in *Proc. IEEE Int. Conf. Robot. Autom.*, Detroit, MI, 1999, pp. 2849–2854.
[2] D. Trivedi, C. Rahn, W. Kier, and I. Walker, "Soft robotics: Biological inspiration, state of the art, and future research," *App. Bionics and Biomech.*, vol. 2, no. 5, pp. 99–117, Jun. 2008.
[3] R. Webster and B. Jones, "Design and kinematic modeling of constant curvature continuum robots: A review," *Int. Jour. Rob. Res.*, vol. 29, no. 13, pp. 1161–1683, Nov. 1969.
[4] I. Walker, D. Dawson, T. Flash, F. Grasso, R. Hanlon, B. Hochner, W. Kier, C. Pagano, C. Rahn, and Q. Zhang, "Continuum robot arms inspired by cephalopods," in *Proc. SPIE Conf. Unmanned Ground Veh. Tech.*, Orlando, FL, 2005, pp. 303–314.
[5] R. Buckingham and A. Graham, "Snaking around a nuclear jungle," *Ind. Robot: An Int. Journal*, vol. 32, no. 2, pp. 120–127, Feb. 2005.
[6] G. Immega and K. Antonelli, "The ksi tentacle manipulator," in *Proc. IEEE Int. Conf. Robot. Autom.*, Nagoya, Japan, 1995, pp. 3149–3154.
[7] D. Lane, B. Davies, G. Robinson, D. O'Brien, J. Sneddon, E. Seaton, and A. Elfstrom, "Practical kinematics for real-time implementation of continuum robots," *IEEE Jour. Ocean. Eng.*, vol. 24, no. 1, pp. 96–111, Jan. 1999.

[8] H. Ohno and S. Hirose, "Design of a slim slime robot and its gait of locomotion," in *Proc. IEEE/RSJ Int. Conf. Intell. Robots Syst.*, Maui, HI, 2001, pp. 707–715.
[9] S. Hirose, *Biologically Inspired Robots*. Oxford, UK: Oxford University Press, 1993.
[10] K. Suzimori, S. Iikura, and H. Tanaka, "Development of a flexible microactuator and its applications to robotic mechanisms," in *Proc. IEEE Int. Conf. Robot. Autom.*, Sacramento, CA, 1991, pp. 1622–1627.
[11] W. McMahan, B. Jones, and I. Walker, "Robotic manipulators inspired by cephalopod limbs," *Eng. Des. Inno.*, vol. 1, no. 2, p. 01P2, Jun. 2005.
[12] G. Chirikjian and J. Burdick, "A modal approach to hyper-redundant manipulator kinematics," *IEEE Trans. Robot. Autom.*, vol. 10, no. 3, pp. 343–354, Jun. 1994.
[13] I. Gravagne and I. Walker, "Kinematics for constrained continuum robots using wavelet decomposition," in *Proc. Conf. and Expo. Robot. for Chall. Situ. and Environ.*, Alburquerque, NM, 2000, pp. 33–38.
[14] B. Jones and I. Walker, "Kinematics of multisection continuum robots," *IEEE Trans. Robot.*, vol. 22, no. 1, pp. 43–57, Feb. 2006.
[15] ——, "Practical kinematics for real-time implementation of continuum robots," *IEEE Trans. Robot.*, vol. 22, no. 6, pp. 1087–1099, Dec. 2006.
[16] G. Chirikjian, "Hyper-redundant manipulator dynamics: A continuum approximation," *Adv. Robot.*, vol. 9, no. 3, pp. 217–243, Jun. 1995.
[17] H. Mochiyama and T. Suzuki, "Kinematics and dynamics of a cable-like hyper-flexible manipulator," in *Proc. IEEE Int. Conf. Robot. Autom.*, Taipei, Taiwan, 2003, pp. 3672–3677.
[18] E. Tatlicioglu, I. Walker, and D. Dawson, "Dynamic modeling for planar extensible continuum robot manipulators," *Int. Jour. Robot. Autom.*, vol. 24, no. 4, pp. 1087–1099, Apr. 2009.
[19] M. Ivanescu and V. Stoian, "A variable structure controller for a tentacle manipulator," in *Proc. IEEE Int. Conf. Robot. Autom.*, Nagoya, Japan, 1995, pp. 3155–3160.
[20] ——, "A controller for hyper-redundant cooperative robots," in *Proc. IEEE/RSJ Int. Conf. Intell. Robots Syst.*, Vanc., Ca., 1998, pp. 167–172.
[21] M. Ivanescu, N. Popescu, and D. Popescu, "A variable length tentacle manipulator control system," in *Proc. IEEE Int. Conf. Robot. Autom.*, Barcelona, Spain, 2005, pp. 3274–3279.
[22] D. Braganza, D. Dawson, I. Walker, and N. Nath, "A neural network controller for continuum robots," *IEEE Trans. Robot.*, vol. 23, no. 6, pp. 1270–1277, Dec. 2006.
[23] A. Kapadia, I. Walker, D. Dawson, and E. Tatlicioglu, "A new approach to extensible continuum robot control using the sliding-mode," *Intl. J. Comp. Tech. and App.*, vol. 2, no. 4, pp. 293–300, 2011.
[24] A. D. Kapadia and I. Walker, "Task space control of extensible continuum manipulators," in *Proc. IEEE/RSJ Int. Conf. Intell. Robots Syst.*, San Francisco, CA, 2011, pp. 1087–1092.
[25] A. D. Kapadia, I. Walker, and E. Tatlicioglu, "Teleoperation control of a redundant continuum manipulator using a non-redundant rigid-link master," in *Proc. IEEE/RSJ Int. Conf. Intell. Robots Syst.*, Algarve, Portugal, 2012, p. accepted to be presented.
[26] J. Burdick, "On the inverse kinematics of redundant manipulators: Characterization of the self-motion manifolds," in *Proc. IEEE Int. Conf. Robot. Autom.*, Scottsdale, AZ, 1989, pp. 264–270.
[27] D. Whitney, "Resolved motion rate control of manipulators and human prostheses," *IEEE Trans. Man Mach. Sys.*, vol. 10, no. 2, pp. 47–53, Jun. 1969.
[28] M. Grissom, V. Chitrakaran, D. Dienno, M. Csencsits, M. Pritts, B. Jones, W. McMahan, D. Dawson, C. Rahn, and I. Walker, "Design and experimental testing of the octarm soft robot manipulator," in *Proc. SPIE Conf. Unmanned Sys. Tech.*, Kissimee, FL, 2006, pp. 109–114.
[29] G. Gallot, O. Ibrahimand, and W. Khalil, "Dynamic modeling and simulation of a 3-d eel-like robot," in *Proc. IEEE Int. Conf. Robot. Autom.*, Rome, Italy, 2007, pp. 1486–1491.
[30] A. Grzesiak, R. Becker, and A. Verl, "The bionic handling assistant - a success story of additive manufacturing," *Assembly Automation*, vol. 31, no. 4, pp. 329–333, Sep. 2011.
[31] Y. Nakamura, *Advanced Robot Redundancy and Optimization*. Reading, MA: Addison-Wesley, 1991.
[32] M. McHenry, "Mechanisms of helical swimming: asymmetries in the morphology, movement and mechanics of larvae of the ascidian *Distaplia occidenalis*," *J. Exp. Bio.*, vol. 204, no. 17, pp. 2959–2973, Sep. 2001.
[33] V. Klema and A. Laub, "The singular value decomposition: Its computation and some applications," *IEEE Trans. Auto. Control*, vol. 25, no. 2, pp. 164–176, Apr. 1980.